Characterization of Sn$_4$P$_3$ film formed by aerosol deposition for lithium-ion battery anode with liquid electrolyte and solid polymer electrolyte

Daiki Azuma, Ryoji Inada*

Department of Electrical and Electronic Information Engineering, Toyohashi University of Technology, 1-1 Hibarigaoka, Tempaku-cho, Toyohashi, Aichi 441-8580, Japan.

*Corresponding author:

Phone: +81-532-44-6723

Fax: +81-532-44-6757

E-mail address: inada.ryoji.qr@tut.jp

Abstract

We fabricated Sn$_4$P$_3$ thin films by aerosol deposition process. Sn$_4$P$_3$ powder pulverized by a ball milling was used as raw material and splayed onto a glass or a stainless steel substrate to form the film via impact consolidation. Electrochemical property as a lithium-ion battery anode was characterized using both an organic liquid electrolyte and poly (ethylene oxide) based solid polymer electrolyte. The initial reversible capacities in both a liquid-type and a solid-polymer cells with a lithium metal as a counter electrode attained to approximately 900 mAh g^{-1}, while the capacity retention of Sn$_4$P$_3$ film electrode after galvanostatic cycling in a cell with a polymer electrolyte was much better than in a cell with a liquid electrolyte. It was also found that the microstructural change of the film after galvanostatic cycling in polymer-type cell is significantly suppressed compared to the film in a liquid-type cell. These results suggest that high-capacity alloy-based anode shows better electrochemical performance in solid-state batteries with deformable solid electrolyte.

Keywords: Tin phosphide; Thin film; Aerosol deposition; Polymer electrolyte; Lithium ion battery anode

1. Introduction

The application field of lithium (Li) ion batteries (LIBs) has been widely spreading from a power source for portable electronic devices to a large-scale one for electric vehicles and plugin hybrid electric vehicles. Along with the expansion of application fields, further improvement of the energy density of LIBs are highly required. Graphite with the theoretical gravimetric capacity of 372 mAh g^{-1} is commonly used current LIB anode. Metallic Li has been recognized as a potential high capacity anode for next-generation rechargeable batteries with higher energy density, because of its high theoretical gravimetric capacity of 3861 mAh g^{-1}, and the most negative standard reduction potential (−3.040 V vs. standard hydrogen electrode) [1]. However, there are several critical issues to be solved for the practical application of Li metal anode such as its high reactivity and non-uniform deposition and dissolution to form Li dendrite and/or dead Li which causes the low coulombic efficiency and safety concerns of batteries. Li alloys such as Li–Si and Li–Sn with a higher theoretical capacity ($Li_{4.4}Si$: 4200 mAh g^{-1}, $Li_{4.4}Sn$: 990 mAh g^{-1}) than graphite with the theoretical capacity of 372 mAh g^{-1} have been extensively studied [2–4], but their poor cycling stability caused by a large volume change during charging and discharging must be overcome for their practical applications. To date, many types of composites including polyphasic alloys and intermetallic compounds have been studied as alternative anode materials for graphite [4–12]. Among these compounds, tin phosphide Sn_4P_3 with the theoretical gravimetric capacity = 1255 mAh g^{-1} is reported as a high capacity alloy-based anode material [9–13]. Sn_4P_3 has a layered crystal structure suitable for Li storage and high intrinsic electric conductivity (= 30.7 S cm^{-1}) at room temperature [13]. Interestingly, Sn_4P_3 is phase-separated into Sn and Li_3P in the Li storage reaction below 1 V vs. Li/Li^+. The latter has good ionic conducting property [13] and would act as a matrix to suppress the volume change during the Li storage reaction [9–11]. Focusing on these features, application of pressed Sn_4P_3 powder anode for ceramic-based all-solid-state batteries has been demonstrated [15], but the cycling stability of pressed Sn_4P_3 powder electrode with solid electrolyte is not discussed in detail.

It is important to examine the applicability of high-capacity alloy-based anode materials for high safety all-solid-state LIBs with high energy density. Difference in the interface formed by an electrode and a liquid or solid electrolyte may influence on the electrochemical performance of an alloy-based

2

anode material. In this work, the electrochemical performance for Sn_4P_3 electrode as a LIB anode was investigated using both an organic liquid electrolyte and a solid polymer electrolyte. For the fabrication of Sn_4P_3 electrode solidified on a metallic substrate, we used the aerosol deposition (AD) methods, which uses impact consolidation for ceramic particles at room temperature [16, 17]. The film formed by AD has similar structural and physical properties as the base powder material and the adhesion strength between the film and a substrate is strong without binders. Based on these features, the applicability of AD process for the rechargeable battery materials have been already investigated [18–34]. Although the initial reversible capacity of Sn_4P_3 film formed by AD attained to 900 mAh g^{-1} using both liquid and polymer electrolyte, the film tested with polymer electrolyte at 60 °C shows much better cycling stability than that tested with a liquid electrolyte at 25 °C. The results suggest that high-capacity alloy-based anode showed better electrochemical performance with a deformable solid electrolyte.

2. Experimental

2.1. Sample preparation

Sn_4P_3 powder was prepared using a mechanochemical synthesis with a planetary ball-milling [8, 9, 19]. Sn (99 %, Kojundo Chemical Laboratory) and amorphous red P (99.9 %, Kojundo Chemical Laboratory, Japan) powders were used as starting materials. Stoichiometric amounts of the starting materials (10 g) were put into a ZrO_2 vessel (45 mL) with ZrO_2 balls with 10 mm in diameter (100 g) and reacted in a planetary ball milling apparatus (Nagao System, Planet M2-3F, Kawasaki, Japan) with a fixed rotation speed of 350 rpm for 8 h under an Ar atmosphere. Then, as-synthesized Sn_4P_3 powder (~10 g) was put into a ZrO_2 vessel with ethanol (30 mL) and ZrO_2 balls with diameters of 1 mm (30 g) and 2 mm (100 g) and pulverized further by a planetary ball-milling at 350 rpm and 16 h. As a result, Sn_4P_3 powder was pulverized to the particle size 0.5–1 μm after ball-milling (Fig. 1(a)), which is suitable for film fabrication via impact consolidation [21].

An AD apparatus consists of a carrier gas supplying system, an aerosol chamber, a deposition chamber equipped with a motored X−Y−Z stage and a nozzle with a thin rectangular-shaped orifice

with the cross-sectional size of 10 mm × 0.5 mm [21, 22, 25]. Ball-milled Sn_4P_3 powder was used as a raw material for fabricating Sn_4P_3 composite film by AD. A carrier nitrogen gas flows out from the gas supply system to the aerosol chamber. In the aerosol chamber, the powder is dispersed into the carrier gas to make an aerosol. Using a pressure difference between the evacuated deposition chamber and the carrier gas system, the aerosol flows into the deposition chamber and is sprayed onto a SUS316L stainless steel or a glass substrate through a nozzle. The deposition area was masked into a square shape with the size of 10 mm × 10 mm. The deposition chamber was evacuated to a low vacuum state at 20–30 Pa and the deposition time was set to 10 minutes. During the deposition process, the stage was moved uni-axially with a back-and-forth motion length of 50 mm and a speed of 10 mm s^{-1}. The distance between the nozzle tip and substrate was set to 10 mm and the mass flow of the N_2 carrier was fixed at 10 L min^{-1}.

2.2. Characterization

The crystal phase of Sn_4P_3 powder and films formed by AD was evaluated by X-ray Diffractometer (XRD; Rigaku, MultiFlex, Tokyo, Japan) using Cu Kα radiation (λ = 0.15418 nm), with a measurement range 2θ of 5–90° and a step interval of 0.02°. Field emission scanning electron microscopy (Hitachi High-Technologies, SU8000 Type II, Tokyo, Japan) was used to observe the size and morphology for powder and film samples. The operation voltage for scanning electron microscope was set to 5 or 10 kV.

Electrical conductivity of Sn_4P_3 film (thickness = 4.5 μm) formed on a glass substrate by AD was evaluated by DC polarization method using a potentio-galvano stat system (VSP-300, BioLogic). Two Au film electrodes with the area size of 16 mm × 5 mm and separation distance of 7 mm were coated on the Sn_4P_3 film formed on a glass substrate by DC sputtering. An applied DC voltage (V) was changed in the range from 10 to 30 mV and the transport current (I) was measured for 5 hours. Measurement temperature was set to 27, 52, 77 and 100 ºC.

Electrochemical properties of Sn_4P_3 film formed on a SUS316L substrate were investigated, using both an organic liquid electrolyte (1 mol L^{-1} LiPF$_6$ in a mixture of ethylene carbonate and dimethyl carbonate with a volume ratio of 1:1 (Kishida Chemical)) and poly (ethylene oxide) based solid polymer electrolyte (Osaka Soda, lithium bis(trifluoromethanesulfonyl)imide / ethylene oxide =

0.06, thickness = 50 μm). The mass loading of Sn_4P_3 film used for electrochemical characterization is ranged from 1.0 to 1.2 mg cm^{-2}. The ionic conductivity of the polymer electrolyte used in this work is 2×10^{-5} S cm^{-1} at 27 °C and 1.6×10^{-4} S cm^{-1} at 60 °C, respectively. A single Li foil serves as both a counter and a reference electrodes. These components were assembled in CR2032 coin-type cells in a dry argon-filled glove box. Celgard 3501 was used as a separator only in the cell with a liquid electrolyte. Using Battery Test System (TOSCAT-3100, TOYO-SYSTEM), galvanostatic charge and discharge testing was carried out at 25 °C for the cell with a liquid electrolyte and 25 and 60 °C for the cells with a polymer electrolyte. The cut-off voltage for electrochemical testing was set to 0–2.5 V.

3. Results and discussion

Figs. 1(b) and (c) show the observation results for the broader surface and transverse cross section of Sn_4P_3 film formed on a SUS316L substrate by AD. The film has a dense structure mainly composed of fractured and deformed Sn_4P_3 particles with the size below 1 μm via room temperature impact consolidation. The film surface seems to be rough but the thickness is confirmed to be approximately 5 μm. Since the total scanning area for AD was 5 cm^2 as mentioned above, the deposition rate per 1 cm^2 area is estimated to be 2.5 μm min^{-1}. Using the theoretical density of Sn_4P_3 (= 5.64 g cm^{-3}), observed film thickness and the film mass per deposition area (= 1.25 mg cm^{-2}), the relative density of Sn_4P_3 film formed by AD is estimated to be approximately 86 %. The XRD patterns of ball-milled Sn_4P_3 powder used for AD and the film formed on a SUS316L substrate are compared in Fig. 1(d). Together with the peaks from a substrate, the peaks from Sn_4P_3 phase are confirmed as the main phase. The peaks from Sn_4P_3 phase in the film become broader and their intensity decreases compared to powder sample, mainly due to the granulation of Sn_4P_3 particles during AD process. The peak observed at 51° (marked with a vertical allow) for film sample is matched with SnO_2 phase but the formation mechanism is not clear.

Fig. 2(a) shows the current-voltage characteristics for Sn_4P_3 film formed on a glass substrate by AD at different fixed temperatures. Linear relation between applied DC voltage and current is clearly observed at each temperature. The slope of data corresponds the electrical resistance and gradually

decreases as the temperature increases, indicating that the conductivity of Sn_4P_3 films increases with temperature. The electrical conductivity along an in-plane direction of Sn_4P_3 film was calculated by the voltage tap separation (= 7 mm) and cross sectional area size of the film (film width = 16 mm, film thickness = 5 μm) and summarized in Fig. 2(b). The room temperature conductivity of Sn_4P_3 film formed by AD is estimated to be 20 S cm^{-1} and much higher than the conductivity of pressed Sn_4P_3 powder sample (= 0.74 S cm^{-1}). This indicates the good connectivity among the Sn_4P_3 particle in the film formed by AD. Although the conductivity of both Sn_4P_3 film and pressed Sn_4P_3 powder are increased slightly with temperature, the change in the conductivity is small.

The change in galvanostatic charge and discharge curves with cycling for Sn_4P_3 film formed by AD with a liquid electrolyte and a solid polymer electrolyte are shown in Fig. 3. It should be noted that the alloying and dealloying reaction of Sn_4P_3 film are defined as charge and discharge reactions in this work. At the first cycle, the charge and discharge capacities of the film electrode in a liquid electrolyte at 25 °C are confirmed to be 960 mAh g^{-1} and 860 mAh g^{-1}, corresponding the initial Coulombic efficiency of 89 % (Fig. 3(a)). The shape of charge and discharge curves for Sn_4P_3 film is very similar with the composite Sn_4P_3 prepared by slurry coating reported in the literature [9−11].

On the other hand, film electrode tested at 25 °C with polymer electrolyte showed electrochemical properties that differed significantly from those in liquid electrolyte (Fig. 3(b)). At initial charge and discharge capacities were only 420 mAh g^{-1} and 300 mAh g^{-1} and from 2nd to 10th cycle, reversible capacity is nearly constant at 200 mAh g^{-1}. After that, an increase in reversible capacity was observed with the passage of cycles up to 20th cycle, and a capacity of 450−500 mAh g^{-1} was obtained at 30−50 cycles. The lower capacity than in liquid electrolyte could be caused by the poor connection at the interface between polymer electrolyte and both Sn_4P_3 film and/or Li metal. In addition, it is presumed that the increase in capacity with the passage of cycles is due to the improvement of the interface.

By increasing the testing temperature to 60 °C, the initial charge and discharge capacities of the film electrode tested with polymer electrolyte are remarkably increased to 1340 mAh g^{-1} and 870 mAh g^{-1} (Fig. 3(b)). Larger charging capacity than the theoretical one for Sn_4P_3 and low efficiency at the first cycle in the film electrode tested with polymer electrolyte at 60 °C are mainly caused by the large

additional capacity observed at the cell voltage of ~1.5 V, probably due to the decomposition of bis(trifluoromethylsulfonyl)imide anion in the polymer electrolyte [35]. From the 2nd cycle onward, the irreversibility in charge and discharge reactions is greatly reduced and the value of efficiency retains 96−98 %, suggesting that the formation of Li^+ conducting solid-electrolyte interphase on the surface of film electrode tested with both electrolytes.

Except for initial few cycles, the shape of charge and discharge curve of the film electrode tested with polymer electrolyte at 60 °C is similar with that with liquid electrolyte, the degradation behavior with cycling is different (Fig. 3(d)). After the 50th cycles at 100 mA g^{-1}, the discharge capacity of the film electrode tested in a liquid electrolyte at 25 °C decreases to 610 mAh g^{-1}, while the film electrode tested with a polymer electrolyte at 60 °C retains higher discharge capacity of 790 mAh g^{-1}. For these two samples, we continued the cycling test further with increasing the current rate to 200, 400, 800 and 1600 mA g^{-1} every five cycles and the results are shown in Fig. 4(a). The typical charge and discharge curves of the film with a polymer electrolyte at different fixed current rates are summarized in Fig. 4(b). It is found that the rate performance for the film electrode tested with a polymer electrolyte inferior to that with a liquid electrolyte, probably due to the lower conductivity in a polymer electrolyte even at 60 ºC than in a liquid electrolyte. However, the recovery of reversible capacity at current rate of 100 mA g^{-1} (at the 71st to 75th cycle in Fig. 4(a)) of the film with a polymer electrolyte is much superior compared to the film tested in a liquid electrolyte. At the 75th cycle, the reversible capacity for the film electrode tested with a liquid electrolyte is degraded to 420 mAh g^{-1}, but the film electrode tested with a polymer electrolyte still maintains higher reversible capacity of 700 mAh g^{-1}.

To discuss further the difference in the cycling stability of Sn_4P_3 films, we took out the film electrodes of the disassembled cells and observed their microstructure. Fig, 5 shows the microstructures of the broader surface of Sn_4P_3 films after cycled with a liquid or a polymer electrolyte. Although all the films were not delaminated from a SUS316L substrate, the structural change of the film by multiple charge and discharge reactions depending on the difference in the types of electrolytes. When polymer electrolyte was peeled off from the cycled Sn_4P_3 film, no debris of sample film adhered to the polymer electrolyte was observed. Therefore, we believe the surface morphology shown in Fig.

5(b) and (c) is true. For the film tested with a liquid electrolyte, the generation of many small cracks and significant agglomeration of the particles are confirmed. The former breaks the electrical conduction path, and the latter reduces to electrochemical utilization of active materials in the film electrode, resulting into acceleration of capacity fading with cycling [21]. On the contrary, we cannot confirm the crack generation in the film tested with a polymer electrolyte at 25 °C and 60 °C, and the particle agglomeration seems to be suppressed remarkably. With changing the testing temperature with polymer electrolyte, slight change of the surface morphology of the films after cycling is confirmed (Fig. 5(b) and (c)). However, there is still large difference between the film tested with liquid electrolyte (Fig. 5(a)) and the film tested with polymer electrolyte at 25 ℃. The polymer electrolyte tightly pressed against the surface of the film electrode would suppress the progress of structural change with cycling, resulting into the higher capacity retention as mentioned above.

4. Conclusion

Using AD process, Sn_4P_3 thin films were formed onto a glass or a stainless steel substrate. High electrical conductivity above 10 S cm^{-1} at room temperature of Sn_4P_3 films formed by AD showed the strong connectivity of Sn_4P_3 particles solidified via impact consolidation. Electrochemical properties as a LIB anode were characterized using both an organic liquid electrolyte and a solid polymer electrolyte. Although the initial reversible capacities obtained with both a liquid or a polymer electrolyte attained to approximately 900 mAh g^{-1}, the capacity retention of Sn_4P_3 film electrode after cycled with a solid polymer electrolyte was much better than with a liquid electrolyte. The change in microstructural of the film after galvanostatic cycling with a polymer electrolyte was significantly suppressed compared to the film cycled with a liquid electrolyte. Although increasing the temperature was necessary to obtain the high capacity with polymer electrolyte in this work, these results suggest that high-capacity alloy-based anode showed better electrochemical performance in solid-state batteries with deformable solid electrolyte.

References

[1]   A. Varzi, K. Thanner, R. Scipioni, D.D. Lecce, J. Hassoun, S. Dörfler, H. Altheus, S. Kaskel, C. Prehal, S.A. Freunberger, Current status and future perspectives of lithium metal batteries, J. Power Sources 480 (2020) 228803.

[2]   M. Winter, J.O. Besenhard, Electrochemical lithiation of tin and tin-based intermetallics and composites, Electrochim. Acta 45 (1999) 31–50.

[3]   U. Kasavajjula, C. Wang, A.J. Appleby, Nano- and bulk-silicon-based insertion anodes for lithium-ion secondary cells, J. Power Sources 163 (2007) 1003–1039.

[4]   W.J. Zhang, A review of the electrochemical performance of alloy anodes for lithium-ion batteries, J. Power Sources 196 (2011) 13–24.

[5]   Y. Idota, T. Kubota, A. Matsufuji, Y. Maekawa, T. Miyasaka, Tin-based amorphous oxide: A high-capacity lithium-ion-storage material, Science 276 (1997) 1395–1397.

[6]   H. Kim, J. Choi, H. Sohn, H. T. Kang, The insertion mechanism of lithium into Mg_2Si anode material for Li-Ion batteries, J. Electrochem. Soc. 146 (1999) 4401–4405.

[7]   R. Yang, X-J. Zhang, T-F. Fan, D-P. Jiang, Q. Wang, Improved electrochemical performance of ternary Sn–Sb–Cu nanospheres as anode materials for lithium-ion batteries, Rare Met. 39 (2020) 1159–1164.

[8]   J-L. Zhang, C-L. Li, W-H. Wang, D. Y. W. Yu, Facile synthesis of hollow Cu_3P for sodium-ion batteries anode, Rare Met. 40 (2021) 3460–3465.

[9]   Y. Kim, C. Lee, T. Kang, H. Sohn, Reaction mechanism of tin phosphide anode by mechanochemical method for lithium secondary batteries, J. Electrochem. Soc. 151 (2004) A933–A937.

[10]   Y. Kim, C. Lee, H. Sohn, T. Kang, Enhancement of capacity and cycle-life of $Sn_{4+\delta}P_3$ ($0 \leq \delta \leq 1$) anode for lithium secondary batteriess, J. Power Sources 141 (2005) 163–166.

[11] B. León, J.I. Corredor, C. Pérez-Vicente, J.L. Tirado, J.L. Tirado, On the mechanism of the electrochemical reaction of tin phosphide with lithium, J. Electrochem. Soc. 153 (2006) A1829–A1834.

[12] W. Wang, J. Zhang, D. Y. W. Yu, Q. Li, Improving the cycling stability of Sn_4P_3 anode for sodium-ion battery, J. Power Sources 364 (2017) 420–425.

[13] J. Liu , W. Sun , Y. Ran , S. Zhou , L. Zhang , A. Wu , H. Huang, Man Yao, Progressive lithiation mechanism of Sn_4P_3 nanosheets as anodes for Li-ion batteries, Appl. Surf. Sci. 550 (2021) 149247.

[14] G. Nazri, Preparation, structure and ionic conductivity of lithium phosphide, Solid State Ionics 34 (1989) 97–102.

[15] A. Ueda, M. Nagao, A. Inoue, A. Hayashi, Y. Seino, T. Ota, M. Tatsumisago, Electrochemical performance of all-solid-state lithium batteries with Sn_4P_3 negative electrode, J. Power Sources 244 (2013) 597–600.

[16] J. Akedo, Room temperature impact consolidation (RTIC) of fine ceramic powder by aerosol deposition method and applications to microdevices, J. Therm. Spray Technol. 17 (2008) 181–198.

[17] D. Hanft, J. Exner, M. Schubert, S. Thomas, P. Fuierer, R. Moos, An overview of the aerosol deposition method: process fundamentals and new trends in materials applications, J. Ceram. Sci. Technol. 6 (2015) 147–182.

[18] H. Usui, Y. Yamamoto, K. Yoshiyama, T. Itoh, H. Sakaguchi, Application of electrolyte using novel ionic liquid to Si thick film anode of Li-ion battery, J. Power Sources 196 (2011) 3911–3915.

[19] H. Usui, M. Shibata, K. Nakai, H. Sakaguchi, Anode properties of thick-film electrodes prepared by gas deposition of Ni-coated Si particles, J. Power Sources 196 (2011) 2143–2148.

[20] H. Usui, T. Sakata, M. Shimizu, H. Sakaguchi, Electrochemical Na-insertion/extraction properties of Sn–P anodes, Electrochemistry 83 (2015) 810–812.

[21] T. Moritaka, Y. Yamashita, T. Tojo, R. Inada, Y. Sakurai, Characterization of Sn_4P_3–carbon composite films for lithium-ion battery anode fabricated by aerosol deposition, Nanomaterials

9 (2019) 1032.

[22] R. Inada, K. Shibukawa, C. Masada, Y. Nakanishi, Y. Sakurai, Characterization of as-deposited $Li_4Ti_5O_{12}$ thin film electrode prepared by aerosol deposition method, J. Power Sources 244 (2014) 181–186.

[23] S. Iwasaki, T. Hamanaka, T. Yamakawa, W.C. West, K. Yamamoto, M. Motoyama, T. Hirayama, Y. Iriyama, Preparation of thick-film $LiNi_{1/3}Co_{1/3}Mn_{1/3}O_2$ electrodes by aerosol deposition and its application to all-solid-state batteries, J. Power Sources 272 (2014) 1086–1090.

[24] T. Kato, S. Iwasaki, Y. Ishii, M. Motoyama, W.C. West, Y. Yamamoto, Y. Iriyama, Preparation of thick-film electrode-solid electrolyte composites on $Li_7La_3Zr_2O_{12}$ and their electrochemical properties, J. Power Sources 303 (2016) 65–72.

[25] R. Inada, T. Okuno, S. Kito, T. Tojo, Y. Sakurai, Properties of lithium trivanadate film electrodes formed on garnet-type oxide solid electrolyte by aerosol deposition, Materials 11 (2018) 1570.

[26] Y. Iriyama, M. Wadaguchi, K. Yoshida, Y. Yamamoto, M. Motoyama, T. Yamamoto, 5V-class bulk-type all-solid-state rechargeable lithium batteries with electrode-solid electrolyte composite electrodes prepared by aerosol deposition, J. Power Sources 385 (2018) 55–61.

[27] T. Yamamoto, H. Iwasaki, Y. Suzuki, M. Sakakura, Y. Fujii, M. Motoyama, Y. Iriyama, A Li-free inverted-stack all-solid-state thin film battery using crystalline cathode material, Electrochem. Commun. 105 (2019) 106494.

[28] M. Sakakura, Y. Suzuki, T. Yamamoto, Y. Yamamoto, M. Motoyama, Y. Iriyama, Low-resistive $LiCoO_2/Li_{1.3}Al_{0.3}Ti_2(PO_4)_3$ interface formation by low-temperature annealing using aerosol deposition, Energy Technol. 9 (2021) 2001059.

[29] D. Popovici, H. Nagai, S. Fujishima, J. Akedo, Preparation of lithium aluminum titanium phosphate electrolytes thick films by aerosol deposition method, J. Am. Ceram. Soc. 94 (2011) 3847–3850.

[30] R. Inada, K. Ishida, M. Tojo, T. Okada, T. Tojo, Y. Sakurai, Properties of aerosol deposited NASICON-type $Li_{1.5}Al_{0.5}Ge_{1.5}(PO_4)_3$ solid electrolyte thin films, Ceram. Internat. 41 (2015) 11136–11142.

[31] D. Hanft, J. Exner, R. Moos, Thick-films of garnet-type lithium ion conductor prepared by the

Aerosol Deposition Method: The role of morphology and annealing treatment on the ionic conductivity, J. Power Sources 361 (2017) 61–69.

[32] R. Inada, T. Okada, A. Bando, T. Tojo, Y. Sakurai, Properties of garnet-type $Li_6La_3ZrTaO_{12}$ solid electrolyte films fabricated by aerosol deposition method, Prog. Nat. Sci. Mater. Internat. 27 (2017) 350–355.

[33] T. Nazarenus, Y. Sun, J. Exner, J. Kita, R. Moos, Powder aerosol deposition as a method to produce garnet-type solid ceramic electrolytes: A study on electrochemical film properties and industrial applications, Energy Technol. 9 (2021) 2100211.

[34] S. Teshima, Y. Ono, N. Goto, R. Inada, Electrical conducting properties of $Na_2Zn_2TeO_6$ thick films fabricated by aerosol deposition, Mater. Lett. 324 (2022) 132640.

[35] K. Yamaguchi, Y. Domi, H. Usui, M. Shimizu, K. Matsumoto, T. Nokami, T. Ito, H. Sakaguchi, Influence of the structure of the anion in an ionic liquid electrolyte on the electrochemical performance of a silicon negative electrode for a lithium-ion battery, J. Power Sources 338 (2017) 103–107.

Figures with captions
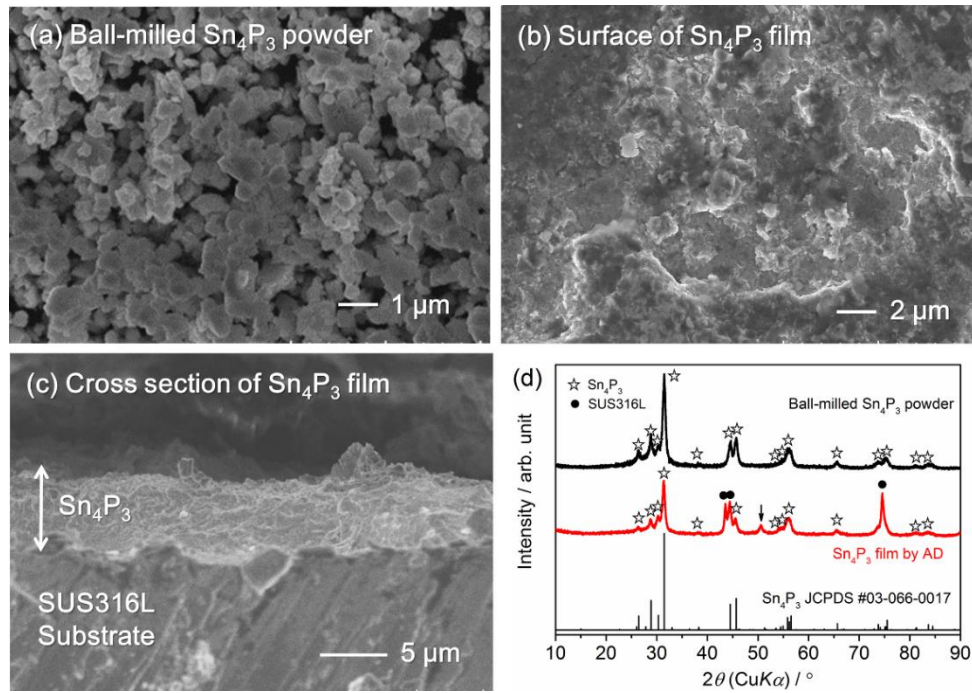
Fig. 1. Observation by scanning electron microscope for (a) ball-milled Sn_4P_3 powder used for film fabrication, (b) the surface and (c) fractured cross section of Sn_4P_3 film formed on a SUS316L substrate by AD. Operation voltages of scanning electron microscope are 10 kV for (a) and 5 kV for (b) and (c). XRD patterns for Sn_4P_3 powders and Sn_4P_3 film on a SUS316L substrate are also shown in (d). The data for film sample is enlarged for readability. The peak marked with a vertical arrow is SnO_2 phase.
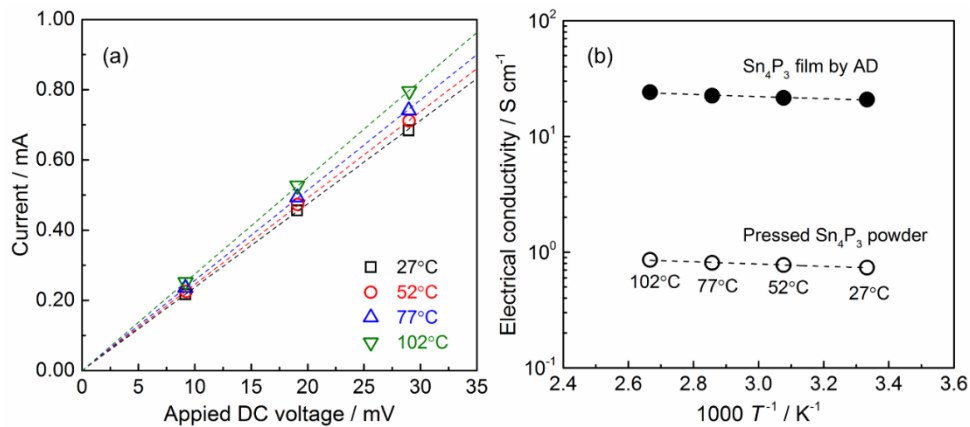
Fig. 2. (a) DC current-voltage characteristics at different temperatures for Sn_4P_3 film (thickness = 4.5 μm) formed on a glass substrate by AD. (b) Electrical conductivity of Sn_4P_3 film and pressed Sn_4P_3 powder plotted against the inverse of temperature. Dashed lines represent the fitting lines for experimental data.
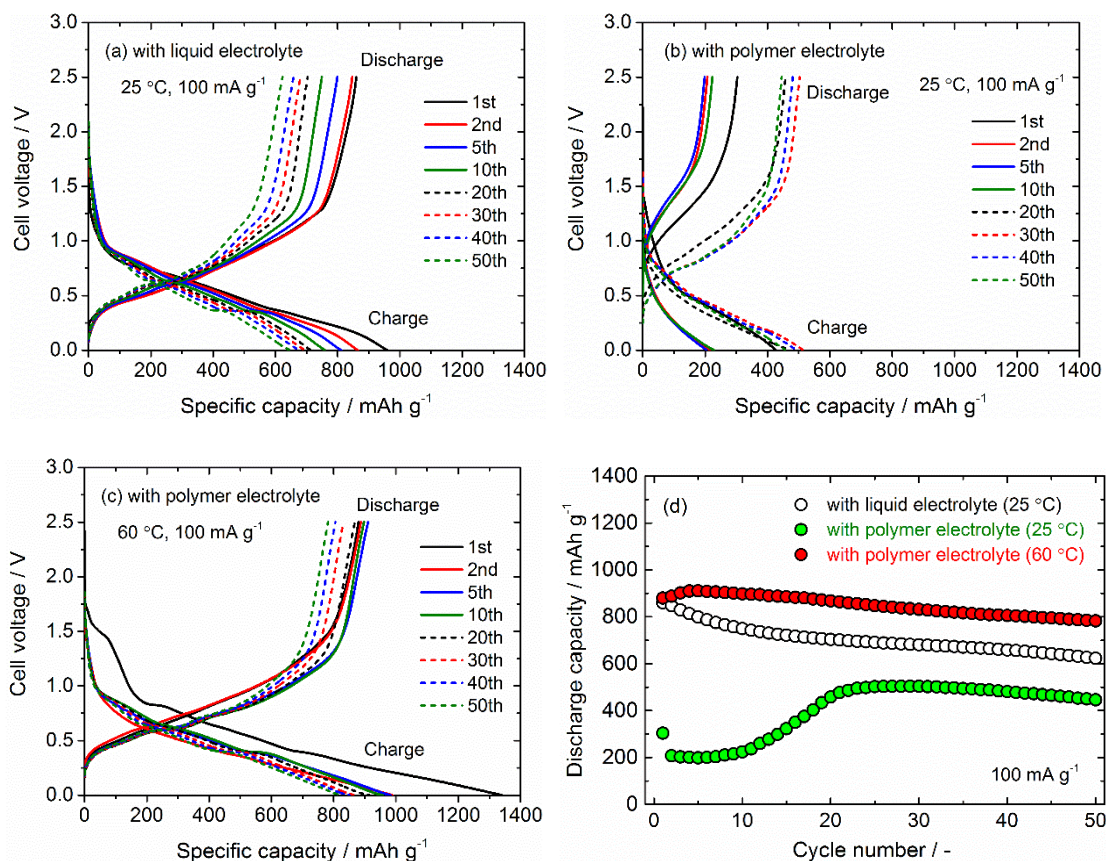
Fig. 3. Galvanostatic charge and discharge curves for Sn_4P_3 film electrodes at current of 100 mA g^{-1}: (a) tested in a cell with an organic liquid electrolyte at 25 ℃, (b) tested in a cell with solid-polymer electrolyte at 25 ℃ and (c) tested in a cell with solid-polymer electrolyte at 60 ℃. Cycling stability for all samples are compared in (d).
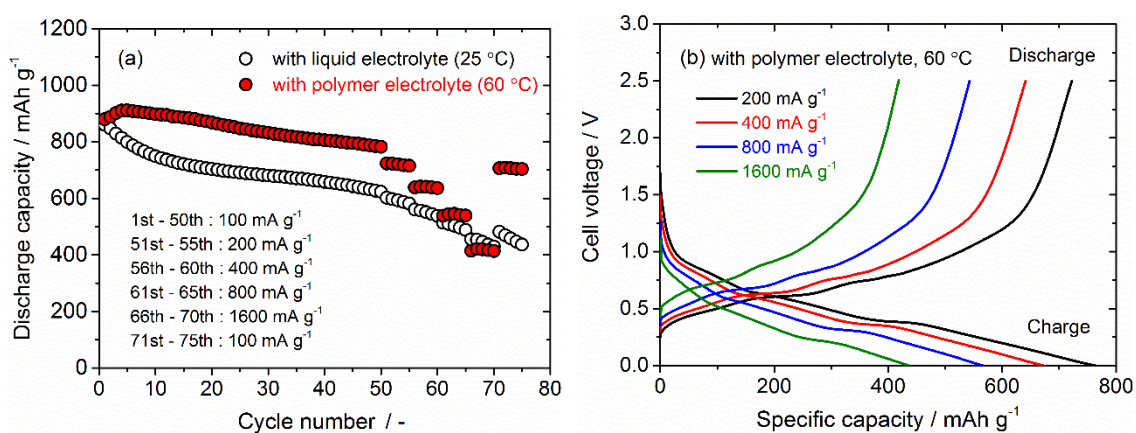
Fig. 4. (a) Comparison of cycling stability at different current densities for Sn_4P_3 film electrodes tested with a liquid electrolyte cell at 25 ℃ and a solid polymer electrolyte cell at 60 ℃. Charge and discharge curves of Sn_4P_3 film electrode with a polymer electrolyte at different fixed currents are shown in (b).
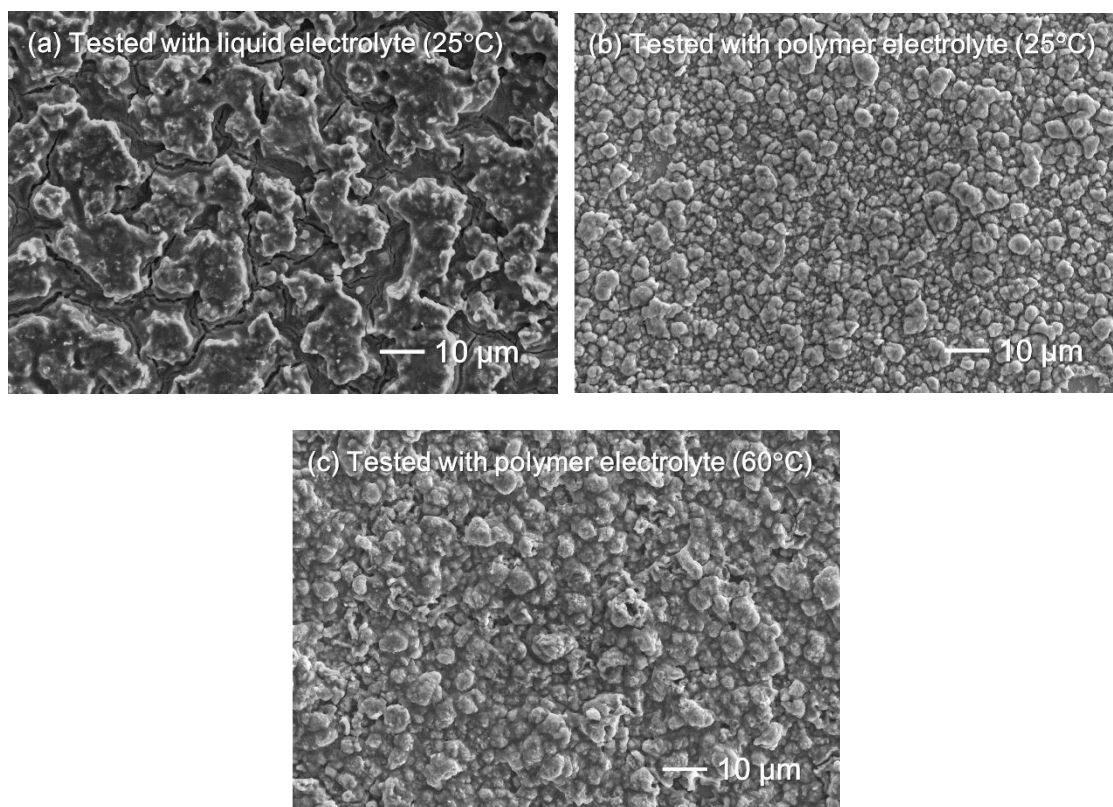
Fig. 5. Surface morphology of Sn$_4$P$_3$ film after galvanostatic cycling test: (a) tested with a liquid electrolyte at 25 ℃, (b) tested with a solid-polymer electrolyte at 25 ℃ and (c) tested with a solid-polymer electrolyte at 60 ℃. Operation voltage of scanning electron microscope is set to 10 kV.